J. Korean Soc. Ind. Appl. Math. Vol.27, No.4, 232–244, 2023 https://doi.org/10.12941/jksiam.2023.27.232

UNSTEADY AERODYNAMICS OF THE STARTING FLOW OF A PLATE OF SMALL ANGLES

SUNG-IK SOHN[1]

[1]DEPARTMENT OF MATHEMATICS, GANGNEUNG-WONJU NATIONAL UNIVERSITY, GANGNEUNG, KOREA
Email address: sohnsi@gwnu.ac.kr

ABSTRACT. The unsteady dynamics of the starting flow of a flat plate is studied by using a vortex shedding model. The model describes the body and separated vortex from the trailing edge of the plate by vortex sheets, retaining a singularity at the leading edge. The model is applied to simulate the flow of an accelerated plate for small angles of attack. For numerical computations, we take two representative cases of the translational velocity of a plate: impulsive translation and uniform acceleration. The model successfully demonstrates the formation of wakes shed from the plate. The wake behind the plate is stronger for a larger angle of attack. Predictions for the lifting force from the model are in agreement with results of Navier-Stokes simulations.

1. INTRODUCTION

The flight of insects and birds has attracted much attention for the past decades owing to its potential applications to micro air vehicles. It has been shown that the conventional aerodynamic theory based on steady flows cannot explain the generation of large lift by small insects, and therefore, unsteady aerodynamics should be considered. Unsteady vortex separation during the thrust stroke of the wing motion plays a crucial role in the production of forces in the flapping flight [1]. At high Reynolds numbers, the diffusion of vorticity is negligible compared with its inertial motion. Thus the evolution of the separated flow can be approximated by the inviscid vortex particles.

The unsteady separated flows are accurately modeled by spiral vortex sheets, where a continuous vortex distribution is shed and advected by the flow. In this approach, both the solid body and separated vortices are described as vortex sheets [2]. Jones [3] developed a model for a moving rigid body and applied it to an accelerating plate with large angles. In this model, a key step in the solution procedure is to impose the unsteady Kutta condition, which regularizes a solution at the edges of the body. Several different forms of the unsteady Kutta condition were presented in this model [2, 3, 4]. The vortex shedding model has been extended to various problems of vortex-body interactions, including falling bodies [5, 6], flapping flags [7],

Received August 13 2023; Revised November 10 2023; Accepted in revised form December 16 2023; Published online December 25 2023.

2020 *Mathematics Subject Classification.* 76B47, 76G25, 76M23.

Key words and phrases. vortex shedding model, vortex sheet, unsteady aerodynamics, starting flow.

hovering and insect flights [8, 9, 10, 11], and fish-like swimming [4, 12, 13]. Note that similar types of vortex shedding model based on the complex conformal mapping [14], or discrete point vortices [15] were also presented.

In this paper, we investigate the unsteady dynamics of an accelerating flat plate for small angles of attack, by using the vortex shedding model. The dynamics of an accelerating plate was previously studied by using this model, but mainly for large angles of attack [3, 16]. In the regime of small angles of attack, the model encounters difficulties in the computation; the leading edge vortex is located close to the body, and the computation becomes unstable. Furthermore, the condition of vortex shedding that moves away from the plate edge is violated, which results in the breakdown of the computation. For these reasons, the computation of the model for small angles of incidence usually suppresses the vortex shedding at the leading edge of a body [6, 13], allowing a singularity there. The circulation at the leading edge is small when the angle of attack is small, and thus the suppression of vortex shedding at the leading edge is a reasonable approximation. Nevertheless, it has not been addressed whether the model under this approximation describes the aerodynamic forces such as lift and drag appropriately. The main purpose of this paper is to validate the model for small angles of attack, by examining the unsteady dynamics of the starting flow including the aerodynamic force.

In Section 2, we describe the inviscid vortex shedding model for an accelerated plate for a small angle of attack. In Section 3, the numerical method of the model is presented. In Section 4, we present numerical results for the starting flow of a plate, for two representative cases of the translational velocity of a plate. Section 5 gives conclusion.

2. VORTEX SHEDDING MODEL

We consider the two-dimensional flow of a flat plate with unsteady translational motion. We assume that the plate is of length $L = 2$ and zero thickness, and the fluid is incompressible inviscid. Figure 1(a) illustrates the flow of vortex shedding of the plate motion in a laboratory frame of reference. At time $t = 0$, the center of the plate is located in $x = 0$ with an angle θ with the x-axis. For $t > 0$, the plate translates with velocity $U(t)$ with a fixed angle.

We assume that free vortex sheet is separated from the trailing edge of the plate, and suppress the vortex shedding at the leading edge. Recall that a vortex sheet is a surface across which the tangential velocity is discontinuous. The plate is also regarded as a bound vortex sheet. The free vortex sheet is denoted by $\zeta_+(\Gamma, t)$ where Γ represents the circulation as a Lagrangian parameter. $\Gamma_+(t)$ denote the total circulation of the free vortex sheet emanating from the trailing edge of the plate. The plate is parameterized by the arc-length s, $-L/2 \le s \le L/2$, and is expressed as

$$\zeta(s, t) = c(t) + se^{\mathrm{i}\theta},$$

where $c(t)$ denotes the location of the center of mass of the plate.

We introduce the body frame of reference which has its origin at the center of mass of the body. (See Fig. 1(b).) The plate in the laboratory frame $\zeta(s, t)$ is related to the body frame

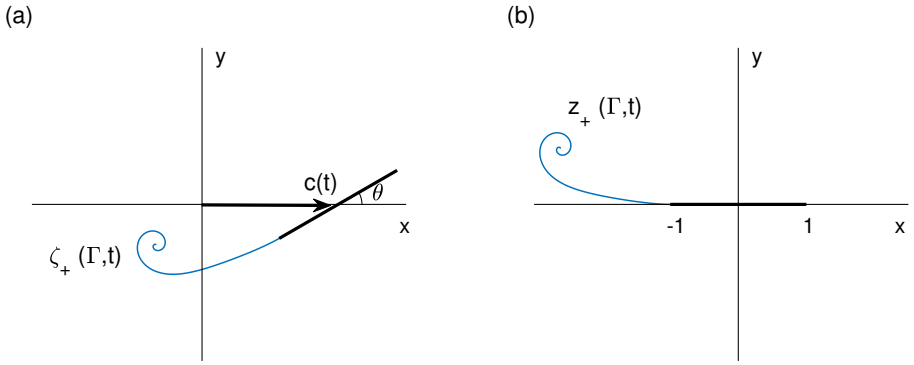

FIGURE 1. Schematic of vortex shedding of a plate: (a) laboratory frame, and (b) body frame

parametrization $s = (\zeta(s,t) - c(t))e^{-\mathrm{i}\theta}$. We denote $z_+(\Gamma,t)$ as the position of the free vortex sheet in the body frame, where they are given by $z_+(\Gamma,t) = (\zeta_+(s,t) - c(t))e^{-\mathrm{i}\theta}$.

2.1. **Equation for free vortex sheet.** The evolution of the free vortex sheet is described by the Birkhoff-Rott equation [17]:

$$\frac{\partial z_+}{\partial t}(\Gamma,t) = \bar{w}(z_+(\Gamma,t),t) - \dot{c}(t)e^{-\mathrm{i}\theta}, \tag{2.1}$$

where $\bar{w}(z,t)$ represents the velocity field in the body frame of reference, and the bar represents the complex conjugate. We define the vortex sheet strength $\gamma(s,t)$ as the jump in the tangential velocity across the bound vortex sheet. The velocity $w(z,t)$ is then expressed as the boundary integral

$$w(z,t) = \frac{1}{2\pi\mathrm{i}}\int_{-1}^{1}\frac{\gamma(\lambda,t)}{\lambda - z}d\lambda + \frac{1}{2\pi\mathrm{i}}\int_{0}^{\Gamma_+(t)} K(z_+(\Lambda,t) - z)d\Lambda, \tag{2.2}$$

where $K(z) = 1/z$ is the singular kernel. The first integral in Eq. (2.2) represents the contribution from the bound vortex sheet, and the second integral represents the contribution from the free vortex sheet. The edge circulation $\Gamma_+(t)$ and the bound vortex sheet strength $\gamma(s,t)$ should be determined as part of the solution.

2.2. **Equations for the edge circulation.** To find the bound vortex sheet strength and edge circulation, we apply the kinematic condition and unsteady Kutta condition. The unsteady Kutta condition is imposed to ensure that the fluid velocity at the edge of the bound vortex sheet remains bounded [3, 4].

The kinematic condition means that fluid does not penetrate the plate on either side. That is to say, the normal component of the fluid velocity on the either side of the body should be the

same as the normal component of the body's velocity. From Jones [4], the kinematic condition gives the following equation:

$$\frac{1}{\pi}\int_{-1}^{1}\frac{\gamma(\lambda,t)}{\lambda-s}d\lambda = f(s,t), \qquad \text{for } -1 \le s \le 1, \tag{2.3}$$

where the right hand side takes the form

$$f(s,t) = 2\nu(s,t) - \frac{1}{\pi}\int_{0}^{\Gamma_+(t)} \mathrm{Re}\left\{K(z_+(\Lambda,t)-s)\right\} d\Lambda. \tag{2.4}$$

Here, $\nu(s,t)$ is the normal component of the velocity of the plate and is given by

$$\nu(s,t) = \mathrm{Im}\{\dot{c}(t)e^{-\mathrm{i}\theta}\}.$$

The integral equation (2.3) can be solved analytically, but the solution is not unique [18]. By imposing the Kutta condition at the trailing edge of the plate,

$$\gamma(-1,t) = 0,$$

we have a solution

$$\gamma(s,t) = -\frac{1}{\pi}\sqrt{\frac{1+s}{1-s}}\int_{-1}^{1}\sqrt{\frac{1-\lambda}{1+\lambda}}\frac{f(\lambda,t)}{\lambda-s}d\lambda.$$

This solution contains an inverse square root singularity at the leading edge of the plate, $s = 1$. We define the bounded part of $\gamma(s,t)$ by

$$\gamma(s,t) = \frac{\sigma(s,t)}{\sqrt{1-s^2}}.$$

Then, the regular part of the solution is expressed as

$$\sigma(s,t) = -\frac{1}{\pi}(1+s)\int_{-1}^{1}\sqrt{\frac{1-\lambda}{1+\lambda}}\frac{f(\lambda,t)}{\lambda-s}d\lambda. \tag{2.5}$$

From the conservation of the total circulation of the flow, we have

$$\int_{-1}^{1}\gamma(s,t)ds = \int_{-1}^{1}\frac{\sigma(s,t)}{\sqrt{1-s^2}}ds = -\Gamma_+(t). \tag{2.6}$$

Then, Eqs. (2.5) and (2.6) give a system of equations for the unknowns $\sigma(s,t)$ and $\Gamma_+(t)$.

2.3. **Force.** The force acting on the body is the pressure difference across the two sides of the plate, since the viscous effects are neglected in our model. Thus, the normal force is expressed as

$$\mathrm{F}(t) = -\mathrm{i}e^{\mathrm{i}\theta}\int_{-1}^{1}[p(\lambda,t)]\,d\lambda,$$

where the square bracket represents the jump across the body. The pressure difference across the two sides of the body is given by

$$[p(s,t)] = -\frac{d\Gamma}{dt}(s,t) - \gamma(s,t)(\mu(s,t)-\tau(t)).$$

Here, $\mu(s,t)$ is the tangential component of the average of the fluid velocities on either side of the body, which is of the form

$$\mu(s,t) = \frac{1}{2\pi}\int_0^{\Gamma_+(t)} \mathrm{Im}\left\{K(z_+(\Lambda,t)-s)\right\} d\Lambda, \tag{2.7}$$

and $\tau(t) = \mathrm{Re}\{\dot{c}(t)e^{-\mathrm{i}\theta}\}$ is the tangential component of the velocity of the body. The circulation on the body is written as

$$\Gamma(s,t) = \Gamma_+(t) + \int_{-1}^{s} \gamma(\lambda,t)d\lambda.$$

3. NUMERICAL METHOD

3.1. **δ-regularization.** The vortex sheet evolution suffers from the Kelvin-Helmholtz instability for all disturbance wavenumbers [17]. It is well known that in a free shear flow, the vortex sheet develops a singularity at finite time. To circumvent the ill-posedness, the vortex blob method in which the singular kernel $K(z) = 1/z$ is replaced by a smoothed kernel [19, 20] is commonly applied. A widely used blob-regularization is to give a constant parameter δ in the kernel,

$$K_\delta(z) = \frac{\bar{z}}{z\bar{z}+\delta^2}.$$

We replace $K(z)$ in Eqs. (2.2), (2.4), and (2.7) by the regularized kernel $K_\delta(z)$. Note that the blob-regularization should not be applied to the bound vortex sheet, because such regularization makes the equation ill-posed. In our simulations, the regularization parameter is set to $\delta/L = 0.1$.

3.2. **Discretization and time integration.** For the discretization of the vortex sheets and the time integration of the equations, we follow a similar procedure as Jones [3] or Shukla and Eldredge [4] and here briefly summarize it. The free and bound vortex sheets are discretized by N lagrangian point vortices. Using the circulation Γ as a Lagrangian variable, we denote the location of the free vortex sheet at the current time t^n by $z_j^n = z_+(\Gamma_j, t^n)$ for $Q+1 \le j \le N$. The Lagrangian indices of the trailing and leading edges of the bound vortex sheet are denoted by the interger P and Q, respectively; here, $P = 1$, because of no vortex shedding at the leading edge. The bound vortex sheet is discretized by using Gauss-Lobatto collocation nodes [3], which are given by

$$s_j = \frac{1}{2}\left[1 - \cos\left(\frac{\pi(j-P)}{Q-P}\right)\right], \qquad P \le j \le Q.$$

The edge circulation is expressed as $\Gamma_Q^n = \Gamma_+(t^n)$.

After discretization, Eqs. (2.5) and (2.6) are combined to determine Γ_Q^n. Then, σ_j^n for $P+1 \le j \le Q$ are obtained, where σ_j^n represents the discrete approximation of the regular part of the bound vortex sheet strength. (Remind $\gamma_Q = \sigma_Q = 0$, and $\gamma_P = \infty$, $\sigma_P < \infty$.) The approximation of the right hand side of Eq. (2.5) involves the integrand with a square

root singularity at the end. A special numerical technique is applied to calculate this quantity with high accuracy. The detail of this technique can be found in the appendix of Shukla and Eldredge [4].

We assume that z_j^n are given at time t^n. At each time step, we first determine Γ_Q^n and σ_j^n by solving Eqs. (2.5) and (2.6), and then calculate the velocity of the free vortex sheet from Eq. (2.1). In Eq. (2.2), the integration over the free vortex sheet is approximated by using the trapezoidal rule, while the integration for the bound vortex sheet is obtained by using the Clenshaw-Curtis quadrature, which is spectrally accurate. Evaluating these quantities, we are ready for time-integration. We employ the classical fourth-order Runge-Kutta method for time-integration to obtain z_j^{n+1}. A new point vortex is released from the trailing edge of the body at the end of each time step.

3.3. **Initial condition.** The solution procedure of the equations requires an initial condition at a time $t_1 > 0$. We use the self-similar solution of the free vortex sheet separated from a plate for the initial condition [3]. A starting point vorticex with zero circulation $\Gamma_N = 0$ is placed initially and its locations z_N is given by the small-time asymptotic expansion of the self-similar solution.

4. RESULTS

We apply the vortex shedding model to the starting flow of a flat plate. We consider the plate velocity of the form $U(t) = t^m$. For numerical computations, we take two cases of the velocity profile, an impulsive translation $U(t) = 1$ and uniform acceleration $U(t) = t$. For both cases, the inclined angle of the plate is chosen as $\theta = 10^\circ$ and 30°, as representative cases for small angles of attack. The number of points is initially set to $N = 62$, and the time step is set to $\Delta t = 0.01$.

4.1. **Impulsive motion.** We first consider the impulsive translational motion $U(t) = 1$. Figures 2 and 3 show the evolution of vortex for the impulsive motion with $\theta = 10^\circ$ and 30°, respectively. For both cases, the trailing edge vortices move little. We find that the vortex for $\theta = 30^\circ$ is stronger than that for $\theta = 10^\circ$. The fine structure of the wake is well resolved by the spiral vortex sheet.

Figure 4 plots the growth of the edge circulation for the impulsive motion with $\theta = 10^\circ$ and 30°. The edge circulation Γ_+ decreases slightly initially and then increases for both cases. The edge circulation for $\theta = 30^\circ$ increases much faster than that for $\theta = 10^\circ$.

We compare the lifting force of the model with results of full numerical simulations. Figure 5 plots the lift coefficient for $\theta = 10^\circ$ and 30°. The lift coefficient is defined as

$$C_L = \frac{2F_y}{\rho U(t)^2 L},$$

where F_y denotes the y-component of the normal force acting on the body, and ρ denotes the density of fluid. In Fig. 5, the solid curve represents the prediction of our model. In Fig. 5(a), the circle represents the result of the viscous vortex particle method for Reynolds number

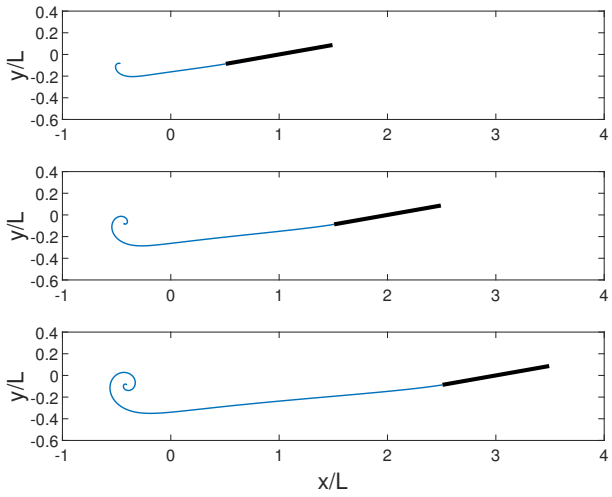

FIGURE 2. Evolution of vortex for the impulsively started plate with $\theta = 10°$. Times are $Ut/L = 1, 2, 3$ from top to bottom.

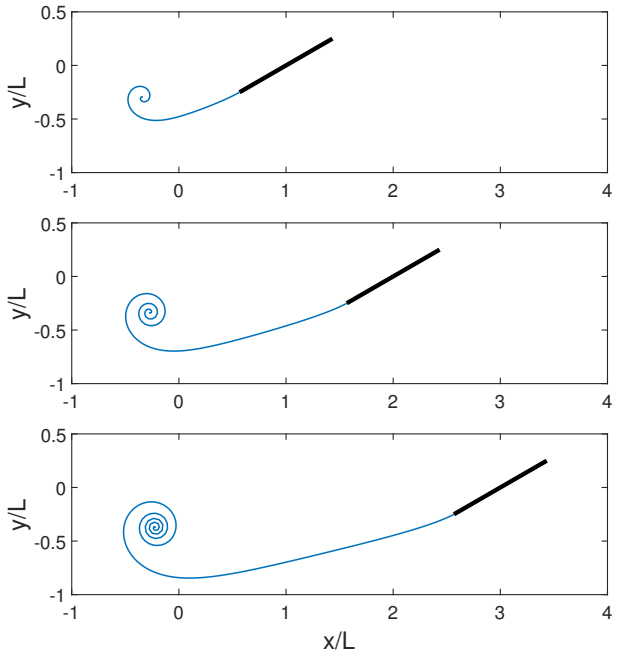

FIGURE 3. Evolution of vortex for the impulsively started plate with $\theta = 30°$. Times are $Ut/L = 1, 2, 3$ from top to bottom.

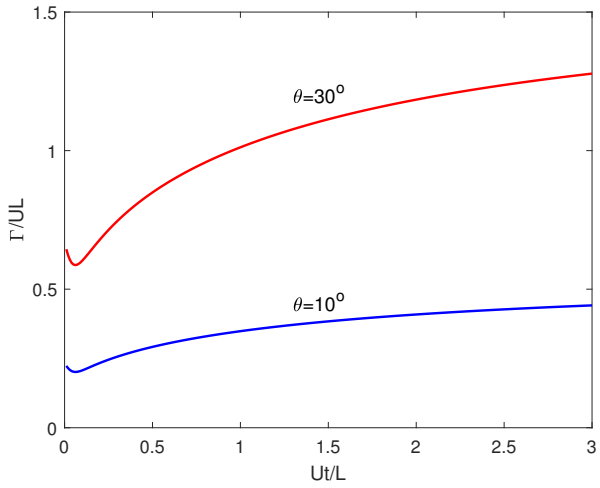

FIGURE 4. Growth of the edge circulation for the impulsively started plate with $\theta = 10^\circ$ and 30°.

$1,000$ by Wang and Eldredge [21]. For $\theta = 10^\circ$, the prediction of the model for lift is in good agreement with the result of the full numerical simulation.

In Fig. 5(b), the circle represents the result of the Navier-Stokes simulation for Reynolds number 200 by Chen *et. al* [22]. For $\theta = 30^\circ$, the lift of the model is in agreement with the result of the full numerical simulation at $t < 2$, but there are some differences between the two results thereafter. These differences may be due to viscous diffusion of vortices of the Navier-Stokes simulation at late times. The agreement of the model with the Navier-Stokes simulation would be better for larger Reynolds number, but that data is not available in the literature. We observe that the lifting force for the plate of $\theta = 30^\circ$ is about three times larger than that for $\theta = 10^\circ$.

4.2. **Motion of uniform acceleration.** We next consider the uniformly accelerated plate with $U(t) = t$. Figure 6 shows the evolution of vortex for the uniformly accelerated plate with $\theta = 10^\circ$ and 30°, at three chord lengths of displacement. We see that the roll-ups of wakes from the uniformly acceleration are weaker than those from the impulsive start in Figs. 2 and 3, at the same chord length.

Figure 7 plots the growth of the edge circulation for the uniformly accelerated plate with $\theta = 10^\circ$ and 30°. Here, we define the dimensionless time as $c(t)/L$, by using chord length of displacement, in order to be generally insensitive to the instantaneous velocity of the plate. In Fig. 7, the edge circulation initially decreases rapidly and then increases. The dimensional circulation is finite at $t = 0$, but the dimensionless circulation becomes infinite, from the scaling by the instantaneous velocity $U(t)$. The circulation for $\theta = 30^\circ$ is much larger than that for $\theta = 10^\circ$, similar to the impulsively started motion.

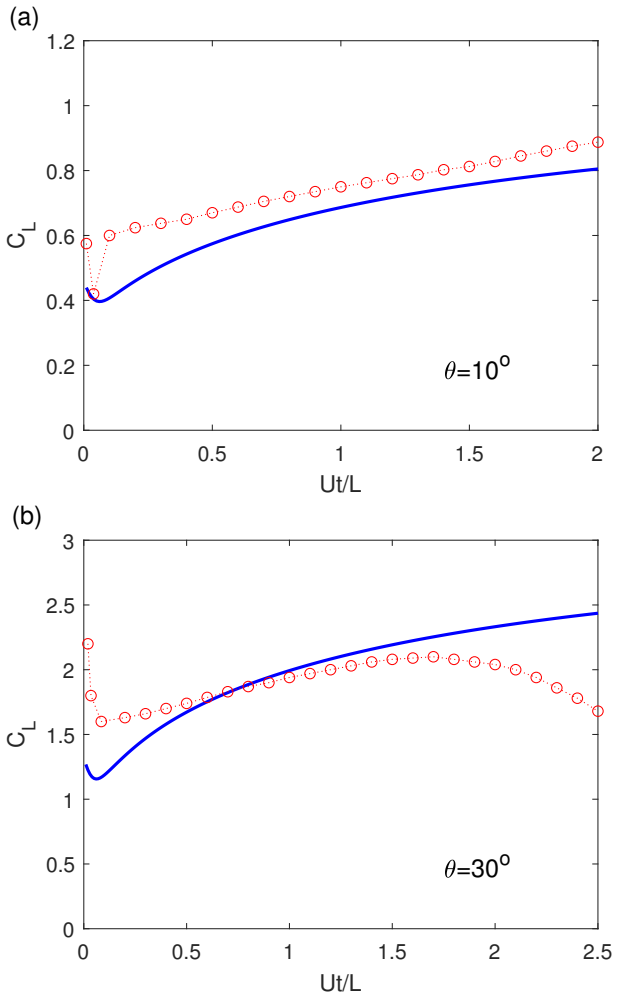

FIGURE 5. Lift coefficient for the impulsively started plate with (a) $\theta = 10^\circ$ and (b) $\theta = 30^\circ$. The solid curve represents the result of our model. In (a), the circle represents the result of the viscous vortex particle method for Reynolds number $1,000$ by Wang and Eldredge [21]. In (b), the circle represents the result of the Navier-Stokes simulation for Reynolds number 200 by Chen *et. al* [22].

Figure 8 shows the lift coefficient for the uniformly accelerated plate for $\theta = 10^\circ$ and 30°. The solid curve represents the prediction of our model. The lift coefficient is infinite at $t = 0$, from the same reason as the dimensionless circulation. The lift coefficient for $\theta = 30^\circ$ is about

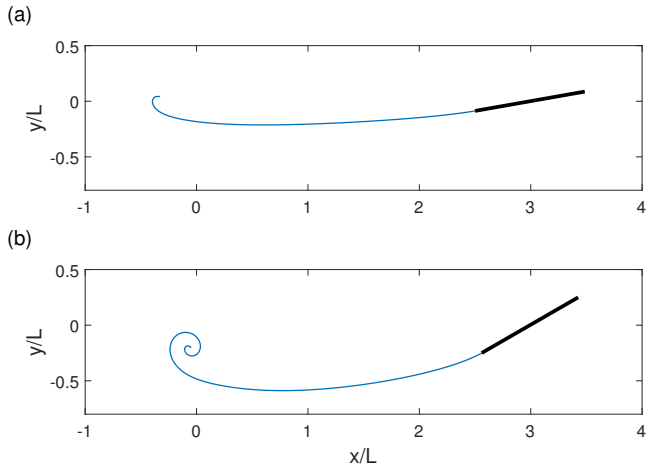

FIGURE 6. Evolution of vortex for the uniformly accelerated plate, at $c(t)/L = 3$. (a) $\theta = 10°$, and (b) $\theta = 30°$.

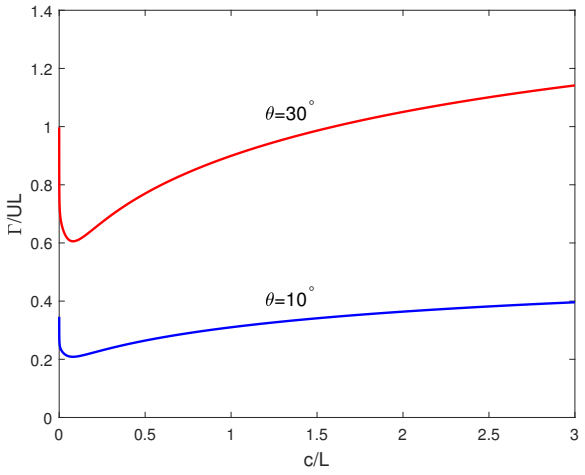

FIGURE 7. Growth of edge circulation for the uniformly accelerated plate with $\theta = 10°$ and $30°$.

twice larger than that for $\theta = 10°$. In Fig. 8, the results of the Navier-Stokes simulation for Reynolds number 100 by Chen *et. al* [22] are also given, which are denoted by circles. They plotted the "augmented lift coefficient" by subtracting the added-mass component from lift. Here, we have readded that component. The lifts of the model agree well with the Navier-Stokes simulations, with the rapid decrease from the infinite force initially.

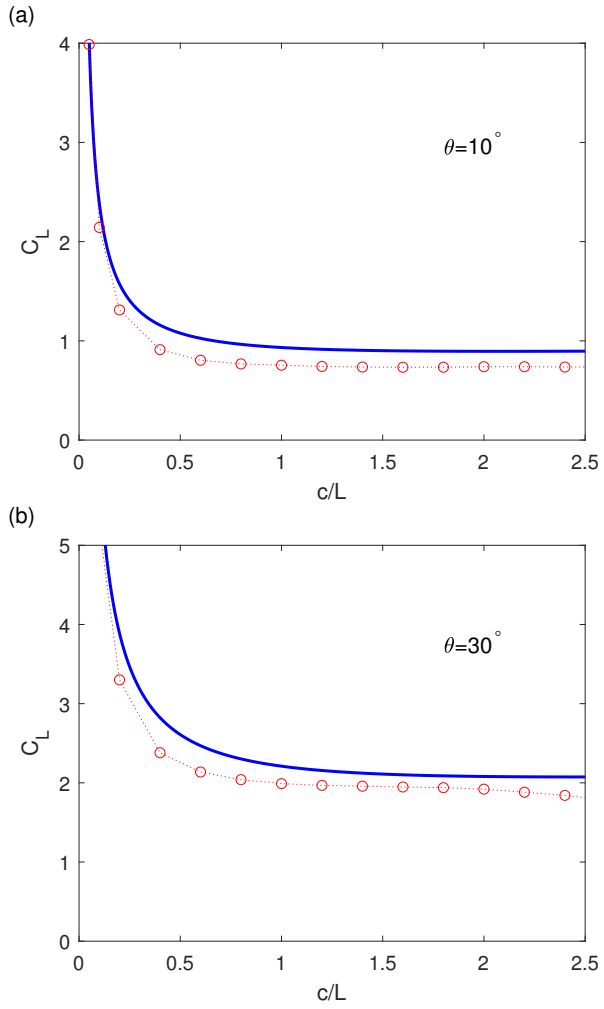

FIGURE 8. Lift coefficient for the uniformly accelerated plate with (a) $\theta = 10^\circ$ and (b) $\theta = 30^\circ$. The solid curve represents the result of our model. The circles represent the results of the Navier-Stokes simulation for Reynolds number 100.

5. CONCLUSION

We have investigated the unsteady dynamics of an accelerated flat plate for small angles of attack by using the vortex shedding model. The model describes the body and separated vortex from the trailing edge by vortex sheets, retaining a singularity at the leading edge. The numerical computation of the model successfully demonstrates the formation of wake shed

from the plate. We find that the wake is stronger for a larger angle of attack, in the flow regime of $\theta \leq 30^\circ$ that we considered.

We have also examined the aerodynamic force acting on the body. The predictions of the model for lift are in agreement with the results of the Navier-Stokes simulations. Therefore, the vortex shedding model which is singular at the leading edge not only qualitatively describes the vortex shedding process of the starting flow for small angles of attack, but also provides a quantitative prediction for the aerodynamic force.

ACKNOWLEDGMENTS

This study was supported by Gangneung-Wonju National University.

REFERENCES

[1] C. P. Ellington, C. van den Berg, A. P. Willmott, and A. L. R. Thomas, *Leading-edge vortices in insect flight*, Nature **384** (1996), 626–630.

[2] M. Nitsche and R. Krasny, *A numerical study of vortex ring formation at the edge of a circular tube*, J. Fluid Mech. **276** (1994), 139–161.

[3] M. A. Jones, *The separated flow of an inviscid fluid around a moving flat plate*, J. Fluid Mech. **496** (2003), 405–441.

[4] R. K. Shukla and J. D. Eldredge, *An inviscid model for vortex shedding from a deforming body*, Theo. Comput. Fluid Dyn. **21** (2007), 343–368.

[5] M. A. Jones and M. J. Shelley, *Falling cards*, J. Fluid Mech. **540** (2005), 393–425.

[6] S. Alben, *Flexible sheets falling in an inviscid fluid*, Phys. Fluids **22** (2010), 061901.

[7] S. Alben and M. J. Shelley, *Flapping states of a flag in an inviscid fluid: bistability and the transition to chaos*, Phys. Rev. Lett. **100** (2008), 074301.

[8] Y. Huang, M. Nitsche, and E. Kanso, *Hovering in oscillatory flows*, J. Fluid Mech. **804** (2016), 531–549.

[9] F. Feng, K. L. Ho, L. Ristroph, and M. J. Shelley, *A computational model of the fight dynamics and aerodynamics of a jellyfish-like fying machine,* J. Fluid Mech. **819** (2017), 621–655.

[10] S.-I. Sohn, *Inviscid vortex shedding model for the clap and fling motion of insect flights*, Phys. Rev. E. **98** (2018), 033105.

[11] Y. Huang, L. Ristroph, M. Luhar, and E. Kanso, *Bistability in the rotational motion of rigid and flexible fyers*, J. Fluid Mech. **849** (2018), 1043–1067.

[12] S. Alben, *Simulating the dynamics of flexible bodies and vortex sheets*, J. Comput. Phys. **228** (2009), 2587–2603.

[13] S.-I. Sohn, *A computational model of the swimming dynamics of a fish-like body in two dimensions*, Phys. Fluids **33** (2021), 121902.

[14] S.-I. Sohn, *An inviscid model of unsteady separated vortical flow for a moving plate*, Theo. Comput. Fluid Dyn. **34** (2020), 187–213.

[15] S. Michelin and S. G. Llewellyn Smith, *An unsteady point vortex method for coupled fluid–solid problems*, Theo. Comput. Fluid Dyn. **23** (2009), 127–153.

[16] L. Xu, M. Nitsche, and R. Krasny, *Computation of the starting vortex flow past a flat plate*, Procedia IUTAM **20**, 2017.

[17] G. Birkhoff, *Helmholtz and Taylor instability*, Proc. Symposia in Applied Mathematics, Vol. XIII, American Mathematical Society, Providence, 1962.

[18] N.I. Muskhelishvili, *Singular integral equations: boundary problems of function theory and their application to mathematical physics*, Wolters-Noordhoff, Groningen, Netherlands, 1958.

[19] R. Krasny, *Desingularization of periodic vortex sheet roll-up*, J. Comput. Phys. **65** (1986), 292–313.
[20] S.-I. Sohn, *Two vortex-blob regularization models for vortex sheet motion*, Phys. Fluids **26** (2014), 044105.
[21] C. Wang and J. D. Eldredge, *Low-order phenomenological modeling of leading-edge vortex formation*, Theo. Comput. Fluid Dyn. **27** (2013), 577–598.
[22] K. K. Chen, T. Colonius, and K. Taira, *The leading-edge vortex and quasisteady vortex shedding on an accelerating plate*, Phys. Fluids **22** (2010), 033601.